Author/s:
Šutka, A;Šutka, A;Dundurs, H;del Rosal, B;Iesalnieks, M;Mālnieks, K;Linarts, A;Barlow, AJ;Leon, RT;Ellis, AV;Sherrell, PC

Title:
Recycled Polystyrene Waste to Triboelectric Nanogenerators: Volumetric Electromechanically Responsive Laminates from Same-Material Contact Electrification

Date:
2024-06-01

Citation:
Šutka, A., Šutka, A., Dundurs, H., del Rosal, B., Iesalnieks, M., Mālnieks, K., Linarts, A., Barlow, A. J., Leon, R. T., Ellis, A. V. & Sherrell, P. C. (2024). Recycled Polystyrene Waste to Triboelectric Nanogenerators: Volumetric Electromechanically Responsive Laminates from Same-Material Contact Electrification. Advanced Energy and Sustainability Research, 5 (6), https://doi.org/10.1002/aesr.202300259.

Persistent Link:
https://hdl.handle.net/11343/351033

ADVANCED ENERGY & SUSTAINABILITY RESEARCH
Open Access
www.advenergysustres.com

Recycled Polystyrene Waste to Triboelectric Nanogenerators: Volumetric Electromechanically Responsive Laminates from Same-Material Contact Electrification

Andris Šutka, Anna Šutka, Henriks Dundurs, Blanca del Rosal, Mairis Iesalnieks, Kaspars Mālnieks, Artis Linarts, Anders J. Barlow, Ronald T. Leon, Amanda V. Ellis, and Peter C. Sherrell**

Millions of tonnes of polystyrene (PS) are produced annually, with only an estimated 12% being recycled. Herein, the upcycling of expanded or foamed PS waste into electromechanically responsive triboelectric laminates (TLs) is described. These TLs possess internal triboelectric dipoles offering an alternative to ferroelectric fluoropolymers, and, when manufactured into triboelectric nanogenerators (TENGs), are able to generate over 200 V and 12 µA from motion. This energy harvesting is enabled by electrospinning alternating layers of small and large diameter PS fibers, which upon friction establish an effective dipole moment within the TL. The PS-TENG shows remarkable stability and is able to charge a 0.47 µF capacitor to 15 V in 200 s of vibration from same material contact electrification, with piezoelectric contact-mode testing showing that a single PS laminate is comparable to state-of-the-art piezoelectric fluoropolymers for overall electromechanical conversion.

1. Introduction

Foamed polystyrene (FPS), also known as extended polystyrene or Styrofoam, is a major environmental problem.[1,2] FPS proliferated and gained worldwide use as a packing material due to perceived advantages over competitor materials.[3] Similar to many synthetic polymers, polystyrene (PS) is slow to biodegrade, with testing showing less than 1% degradation over 90 days,[4] being "essentially inert" in landfill.[5] FPS is extremely light, with a density of 11–50 kg m^{-3}, with approximately 95% air content, meaning it has a large volume-to-mass ratio, making storing or shipping economically prohibitive. These challenges in packing and transportation of FPS waste have led to only a very small percentage of it being recycled. While the FPS industry estimates 12% of all FPS is recycled, government estimates place the value below 1%.[6] This is despite FPS being easily recyclable in a range of green solvents,[7] or by catalytic pathways.[8] Quite simply, it is economically more viable to create new FPS than to recycle existing FPS.[9] Thus, developing routes to produce valuable products from recycled PS can provide an additional imperative to help address burgeoning PS waste.[10]

The internet of things (IoT) requires low-cost, recyclable, and efficient energy sources for remote and autonomous sensing

A. Šutka, A. Šutka, H. Dundurs, M. Iesalnieks, K. Mālnieks
Institute for Materials & Surface Engineering
Faculty of Natural Sciences and Technology
Riga Technical University
Paula Valdena 3/7, Riga LV-1048, Latvia
E-mail: andris.sutka@rtu.lv

B. del Rosal
School of Science
RMIT University
Victoria 3000, Australia

DOI: 10.1002/aesr.202300259

A. Linarts
Institute of Technical Physics
Faculty of Natural Sciences and Technology
Riga Technical University
Paula Valdena 3/7, Riga LV-1048, Latvia

A. J. Barlow, R. T. Leon, A. V. Ellis, P. C. Sherrell
Department of Chemical Engineering
The University of Melbourne
Parkville 3010, Victoria, Australia
E-mail: peter.sherrell@rmit.edu.au

A. J. Barlow
Materials Characterisation and Fabrication Platform
The University of Melbourne
Parkville 3010, Victoria, Australia

P. C. Sherrell
Applied Chemistry & Environmental Science
School of Science
RMIT University
Victoria 3000, Australia

systems.[11,12] Currently, motion can be used to power IoT devices via piezoelectric fluoropolymers; however, the environmental impact of fluoropolymer synthesis and degradation has led to governments globally moving to ban fluoropolymer production.[13–15] Triboelectric nanogenerators (TENGs), have emerged as exceptionally promising devices for converting low frequency, ambient movement, or vibration, into electricity.[16–18] TENGs consist of two polymer surfaces that periodically undergo contact separation, resulting in one polymer surface gaining a positive charge, and one polymer surface gaining a negative charge.[19]

Historically, it was believed that the two polymer surfaces within a TENG needed to have different polymer chemistries; however, research has since demonstrated that same-material contact electrification can occur if the two polymer surfaces have different topographical or deformative properties.[20–24] Notably, smooth surfaces in same-material contact electrification were demonstrated to preferentially charge negatively compared to relatively rougher, high aspect ratio, surfaces.[23] Despite these advances, same-material TENGs have suffered from lower energy outputs compared to conventional TENGs, simply due to a comparative lack of driving force for charge separation.[25] This lower energy output has meant for practical applications, same-material TENGs have not been widely adopted or studied. Further, TENGs traditionally require macroscopic contact separation to function and thus do not generate electricity in a single material analogous to a piezoelectric polymer film.

Recently, laminates produced from alternating distinct polymers have been developed to introduce internal friction interfaces within a filmlike polymer patch.[26,27] These laminates exhibit volumetric charging having the same response of piezoelectric materials, from polymers with centrosymmetric crystal structures. The introduction of volumetric charging into TENGs has theoretically enabled a dramatic improvement in energy conversion from any TENG structure, enabling bulk (as opposed to surface) charging of the polymer mat or laminate.[26,27] These laminates function by controlling the interlayer adhesion within an assembly of polymer bilayers, with the polarity of the internal triboelectric dipoles arising from a combination of asymmetric triboelectric cohesive energy density[28] and roughness (fiber diameter) effects.[23]

Here, for the first time, we demonstrate a laminate which functions through "same-material" contact electrification. At the same time, these concepts are used to introduce electromechanical response into a recycled waste material, FPS. While the authors note that TENGs from electrospinning have been created before,[29,30] none have been produced with an internal volumetric electromechanical response. The production of these laminates from recycled FPS was demonstrated, and the electromechanical response of these laminates was assessed. The PS

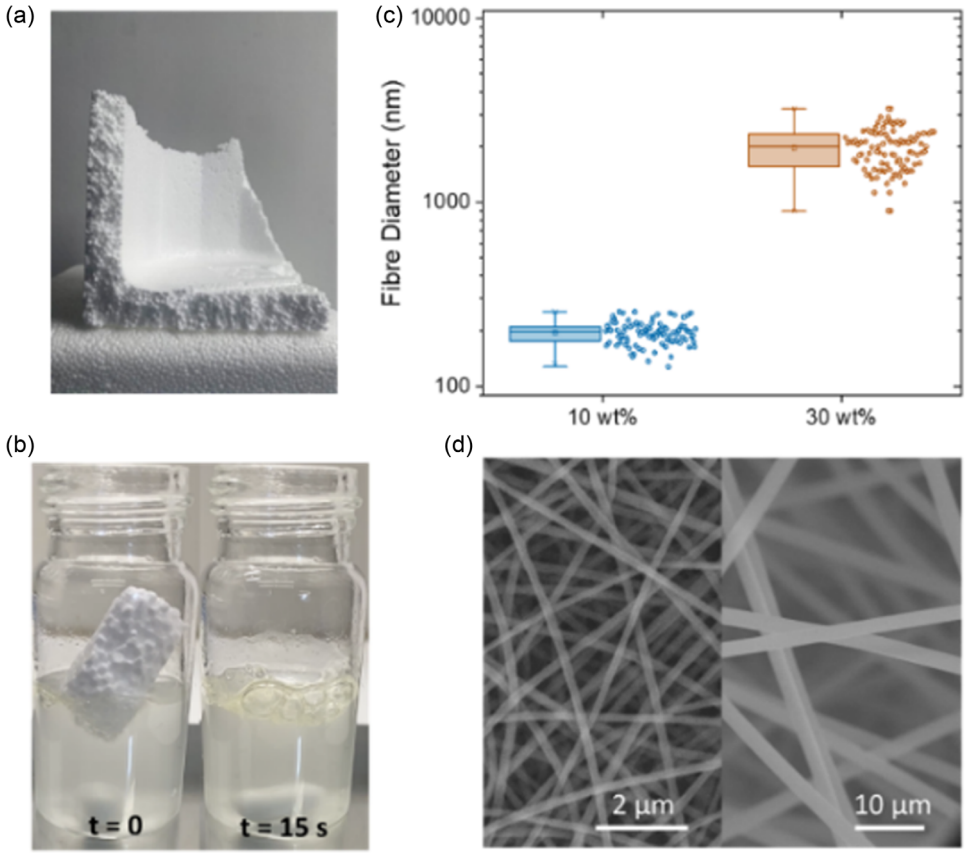

Figure 1. Recycling and electrospinning of FPS fibers; a) raw FPS material; b) dissolution of FPS in 0.15:1 v v^{-1} THF/DMF solution over 15 s; c) fiber diameter from 10 to 30 wt% FPS solutions ($N = 200$); and d) scanning electron microscopy (SEM) images and diameter distribution for electrospun recycled PS small- and large-diameter fibers.

laminates are fabricated from alternating layers of small-diameter (200 ± 30 nm) and large-diameter (2000 ± 500 nm) electrospun PS fibers. This work provides a pathway for preparing piezoelectric-like electromechanically responsive materials from a single non-ferroelectric polymer—FPS. Recycling FPS into high added value products (alternative energy harvesters), providing an impetus to decrease the environmental burden from FPS and may lead to electromechanically responsive polymers without the environmental burden of fluoropolymers.

2. Results and Discussion

2.1. Recycling and Processing Polystyrene: Making Laminates

FPS waste was sourced from equipment packaging (**Figure 1**a), and was manually broken and dissolved in 0.15:1 v v^{-1} tetrahydrofuran (THF):*N*,*N*-dimethylformamide (DMF) solution within 15 s (Figure 1b). These solutions of the dissolved FPS (10 and 30 wt%) were directly electrospun to produce fibers of different diameters (Figure 1c,d, Figure S1, Supporting Information), 200 ± 30 nm for the 10 wt% solution and 2000 ± 500 nm for the 30 wt% solution. These diameters were chosen to be an order of magnitude apart for the creation of fixed and slip interfaces which will be discussed later. The authors also note that FPS may contain non-polystrene additives, dependent on local source; however these will be homogenously during dissolution and electrospinning through the fibers, and thus will not affect the final product.

By alternating the feedstock solution between 10 and 30 wt% FPS solution a layer-by-layer assembly of laminate structure was produced (**Figure 2**a–c). As described by Linarts et al.[26] such an alternating assembly of large–small fibers leads to the creation of fixed and slip interfaces (as described later), while also providing the asymmetric roughness properties (from contact between "smooth" (large) and "rough" (small) features)[23] to enable contact electrification.

To create a fixed interface, 200 nm diameter fibers were electrospun on a mat of 2000 nm diameter fibers. These 200 nm diameter fibers were found to penetrate the existing pore network of the 2000 nm diameter fiber layer and thus have strong interfacial adhesion. In contrast, a slip interface was created when 2000 nm diameter fibers were electrospun onto a densely packed array of 200 nm diameter fibers. Here, the 2000 nm diameter fibers could not penetrate the pores of the 200 nm diameter fiber layer, only sitting on the surface and thus having a poor interlayer adhesion. To quantify this difference in adhesion, a vertical peel test was performed (Figure 2d,e). When 2000 nm diameter fibers were electrospun on a fiber layer consisting of 200 nm diameter fibers, the average interlayer adhesion was measured as 0.018 ± 0.009 mN, with a maximum adhesive force of 0.039 mN. In contrast, when the 200 nm diameter fibers were electrospun on a fiber layer consisting of 2000 nm diameter fibers, the average adhesion was threefold larger at 0.06 ± 0.02 mN, with a maximum adhesive force of 0.12 mN. This difference between interfacial adhesive force enabled slip to preferentially occur between large-diameter fibers electrospun on top of small-diameter fibers.

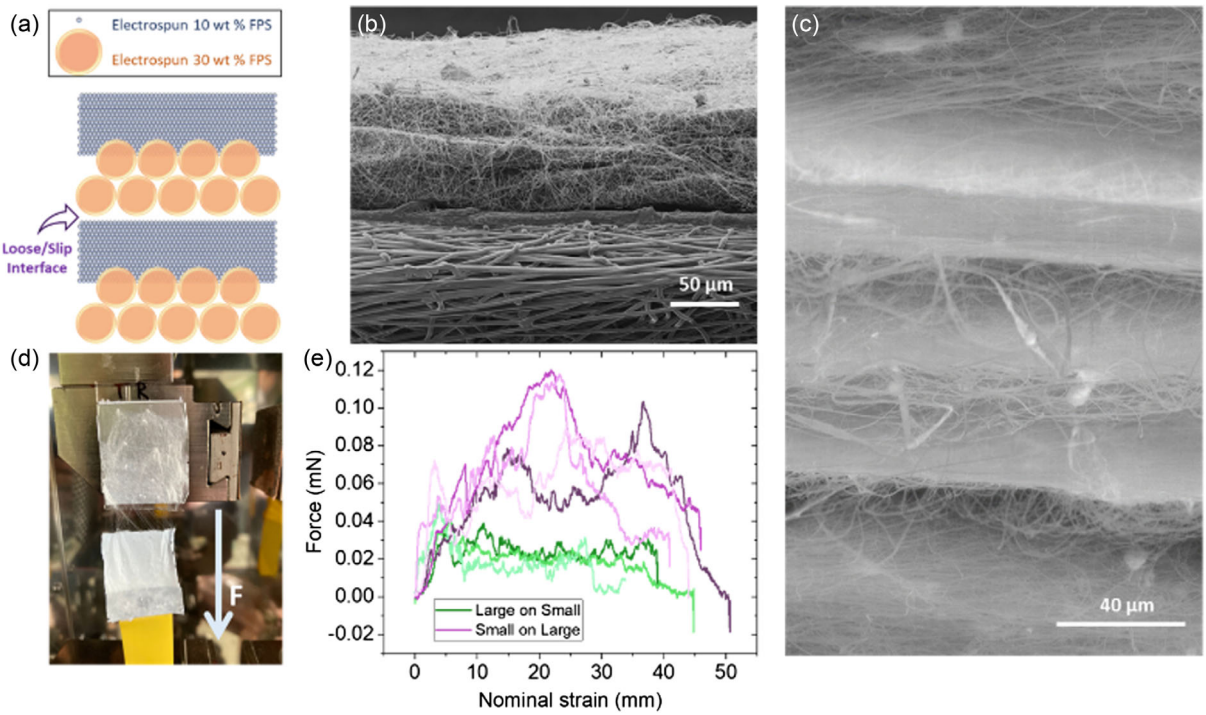

Figure 2. a) An idealized schematic showing tightly bound versus loose/slip interfaces; b) HIM of a cryo-ion mill cut bilayer recycled polystyrene (rPS) laminate, showing the fiber ordering of the layers; c) cross-sectional SEM image of a 15-bilayer rPS laminate; d) photograph of the peel testing configuration for testing the interlayer adhesion between fiber layers; and e) force required to maintain a constant strain rate of 1.66 mm s^{-1} when delaminating FPS 30 wt% solution-spun fibers (large diameter) on FPS 10 wt% solution-spun fibers (small diameter), and small-diameter fibers spun on large fibers.

Controlling the formation of the slip and fixed interfaces, led to the recycled polystyrene (rPS) laminate demonstrating an electromechanical response. When a three-bilayer rPS laminate was tested under cyclic compression testing, a clear current and voltage response was observed (**Figure 3**a)—showing electricity production from motion from purely polystyrene interfaces. Manually assembling three-bilayer laminates with misaligned interfaces produced no electrical response from the cyclic compression testing (Figure 3c). Similarly, manually assembling six layers of fibers (thus eliminating fixed interfaces) resulted in negligible electrical production (Figure 3c). In comparison, the creation of alternating fixed-slip interfaces resulted in a 122×-fold enhancement in voltage output compared to an equivalent assembly with no fixed interfaces.

The authors note that while electrospinning will induce charges on the fibers "as-spun,"[31] these electrospinning generated surface charges have diminish overtime, as shown by minimal electromechanical conversion observed in Figure 3b,c. In particular, it would be expected that Figure 3c would show the same electromechancial conversion as Figure 3a if the electrospinning charges played a role. Instead, contact-electrification-produced surface charges from friction at the slip interface driven by heterolytic bond cleavage and charge transfer lead to the observed electrochemical conversion.

It is important to note that the current and voltage measured arise purely from contact electrification arising from the difference in fiber topography (diameter), and not any difference in surface chemistry as all materials were spun from equivalent solutions at different FPS concentration in THF/DMF, this is termed same-material contact electrification and has been observed by ourselves,[23,32] and others.[20,21,25,33]

To understand how the introduction of a fixed interface leads to mechanical-to-electrical energy conversion, the polarity across multiple interfaces should be considered. As the rPS laminate is compressed, there is slip between large and small fibers and the slip interface, generating negative charge on large, smooth fibers and positive charge on small fibers, creating a triboelectric dipole.[5,23] As the force is released and reapplied, the oscillating dipoles lead to the measured voltage output, represented schematically in **Figure 4**a,b. When no fixed interface is introduced, into the rPS laminate (by manual assembly of individual layers), this charging phenomena occurs on both sides of each small and

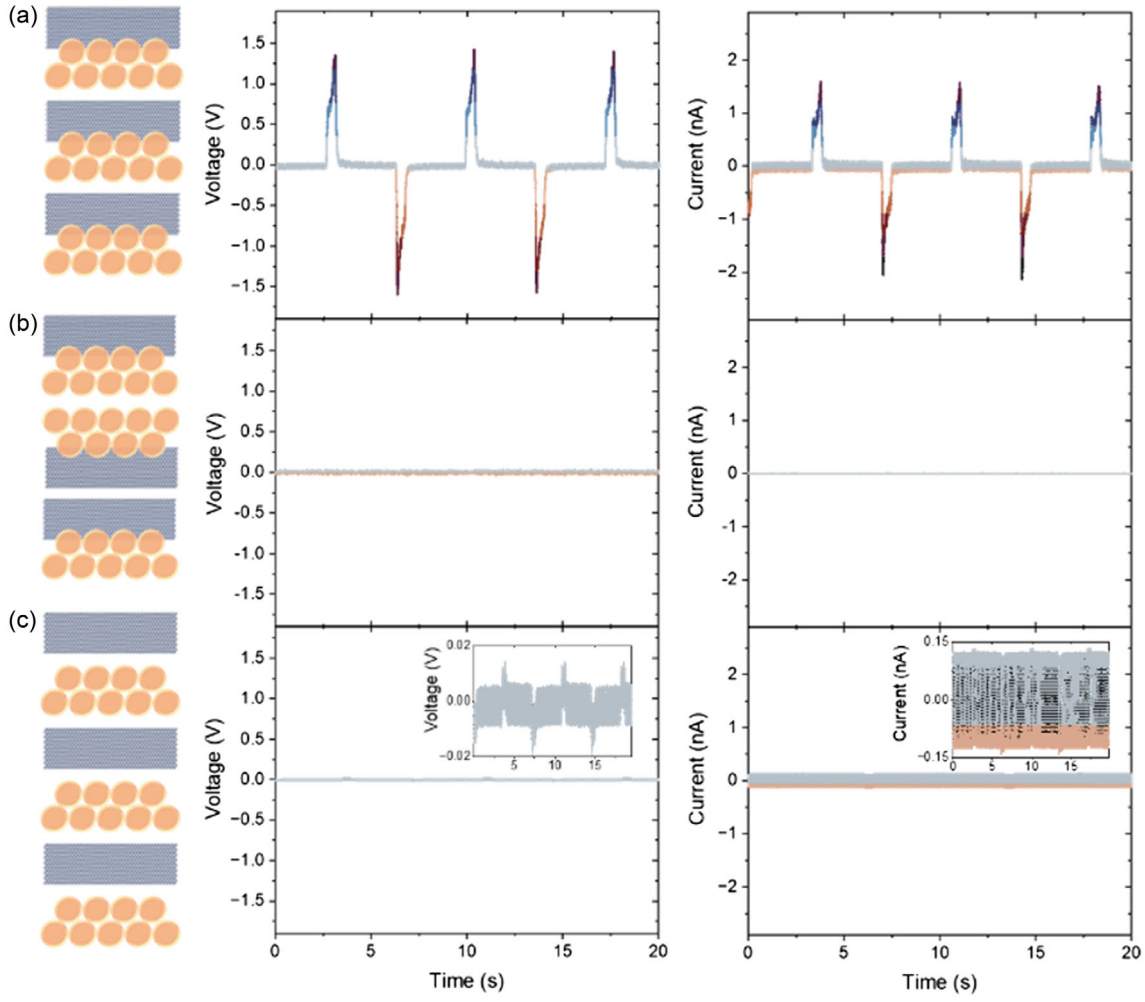

Figure 3. Electromechanical voltage and current output from electrospun rPS laminates under 2–12 N cyclic compression; a) three bilayers with alternating fixed-slip interfaces; b) three bilayers with unordered fixed-slip interfaces; and c) six layers assembled manually to remove any fixed interfaces.

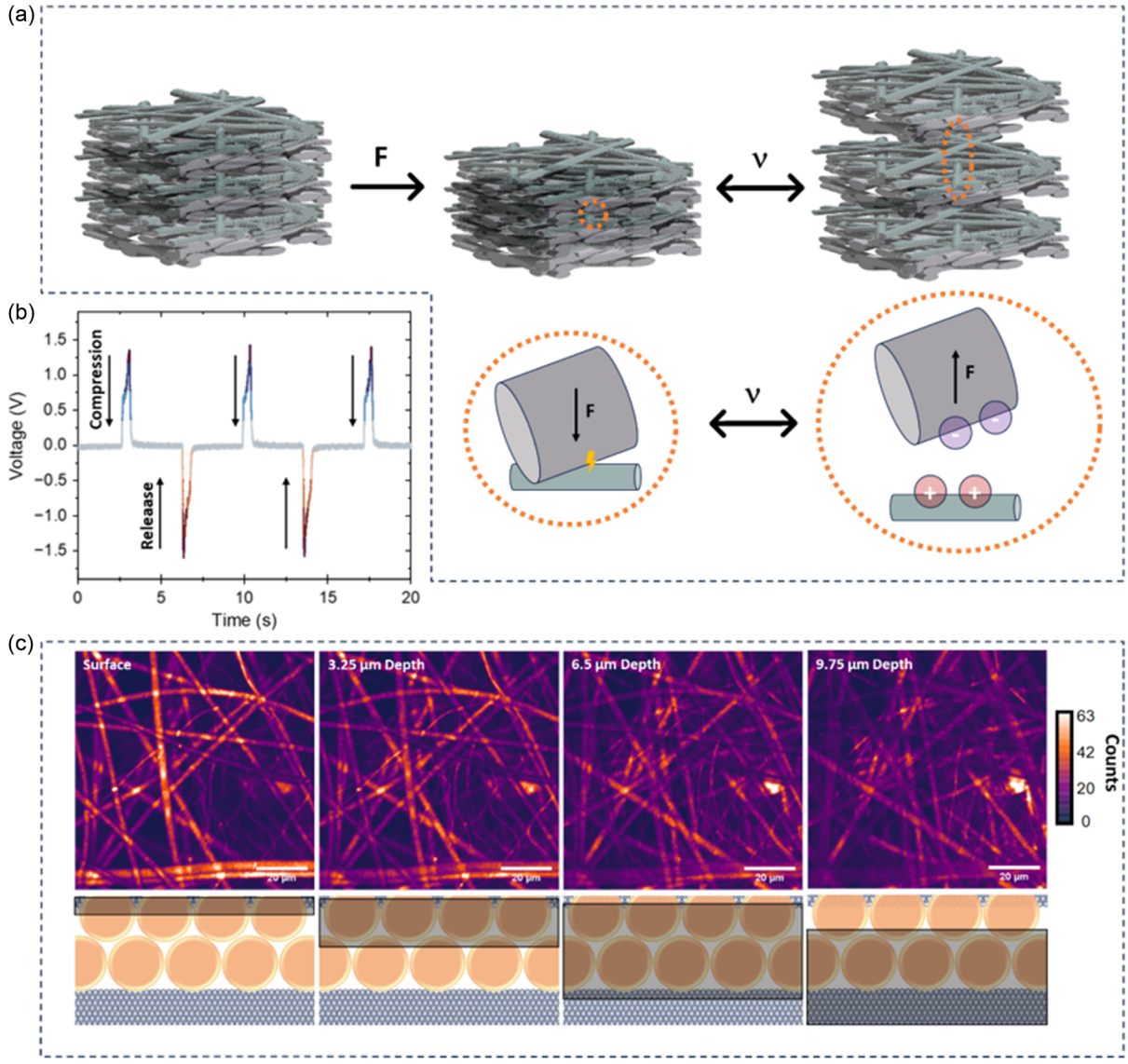

Figure 4. a) Schematic (not to scale) demonstrating slip between large and small fibers during compression leading to individual charging events generating a triboelectric dipole, and subsequent macroscopic mechanical-to-electrical conversion; b) voltage generated from cyclic compression at between 2 and 12 N ($\Delta F = 10$ N) of an aligned three-bilayer rPS stack; and c) coherent anti-Stokes Raman scattering of rPS laminates; the images show the epi-CARS signal collected at increasing Z depths in a 30-bilayer structure, with the region appearing in the epi-CARS signal shown by the schematics below each surface.

each large layer. In this case, the internal dipoles fully cancel out and no external electricity can be harvested from the rPS laminate.

Confocal anti-Stokes Raman spectroscopy (CARS) was used to visualize the internal interfaces within a rPS laminate (Figure 4c). The CARS volume maps revealed a clear transition between an interface containing mixed small- and large-diameter fibers and a layer of large-diameter fibers, providing clear evidence of the intermixing between small- and large-diameter fibers across the fixed interface (Figure 4c); for a full description of the CARS interpretation, please see Supporting Information.

Thus far, we have shown the proof of principle in creating electromechanically responsive rPS laminates; in the following sections, we will explore scaling these rPS laminates as pseudo-piezoelectric materials and for TENGs.

2.2. Electromechanical Performance: Piezoelectric Mode

We have previously demonstrated for non-recycled materials that the triboelectric charge increased linearly with increasing triboelectric interfaces in the laminate.[26] To maximize energy-harvesting performance, rPS laminate structures were scaled from 3 bilayers up to 30 bilayers (60 layers) with the same total thickness of ≈300 μm. The 30-bilayer structure was chosen as the maximum layer number (to maximize generated surface

charge) maintains a 300 μm thickness while containing 2000 ± 500 nm fibers.

Cyclic compressive testing of the 30-bilayer laminate (**Figure 5**a) was performed to assess the electromechanical response of the rPS laminate. These tests were performed in contact or "piezoelectric" mode (Figure 5b), where there is no separation between the mechanical tester and sample during cyclic compression. This is achieved by applying a preload force, in this case 2 N, with the testing load ($\Delta F = 10$ N) applied to measure electromechanical response. The peak-to-peak short-circuit current (I_{sc}) was measured 6.1 ± 0.2 nA (Figure 5c-i) while the peak-to-peak open-circuit voltage (V_{oc}) was measured to be 23.5 ± 0.1 V (Figure 5c-ii). The peak-to-peak voltage output of 23.5 V was comparable, or higher, than equivalent voltage outputs from state-of-the-art fluoropolymer piezoelectric nanogenerators with an equivalent 10 N of force (**Table 1**).[34–45]

While higher voltage and current values have been reported in literature for piezoelectric fluoropolymer composites,[46] these are with uncontrolled testing parameters (such as finger tapping or palm tapping) which cannot be benchmarked.[34] Here, the electromechanical response of the rPS laminate was proved to arise from the internal triboelectric interfaces within the rPS laminate by the fast Fourier transform technique, which showed a significant bandwidth indicative of triboelectric interfaces (Figure S2, Supporting Information).[47]

The applicability of the rPS laminates as a vibrational energy harvester was demonstrated by varying air pressure air applied onto the rPS laminate (**Figure 6**a). The air pressure on one side of the laminate was oscillated at 14–15 Hz between the edge and center of the rPS laminate (Video S1, Supporting Information), while on the back side, the air pressure was kept in a constant location. When this experiment was performed on a dense polystyrene film, negligible current was measured (<0.005 μA) (Figure 6b); however, the 30-bilayer rPS laminate showed >2 μA of current, which was constant over 40 000 cycles (Figure 4c).

Table 1. Comparison of piezoelectric-polymer-based voltage outputs for piezoelectric mode testing compared to rPS laminates.

Material	ΔF	f	V_{p-p}	References
Polyvinylidene difluoride (PVDF)–Lead zirconate titanate	10 N	1.5 Hz	2.3 V	[45]
Porous PVDF	20 N	0.8 Hz	12 V	[44]
$Bi_{3.15}Nd_{0.85}Ti_3O_{12}$/poly(vinylidene fluoride-co-hexafluoropropylene)	10 N	2.0 Hz	40 V	[40]
$Bi_{0.5}Na_{0.5}TiO_3$/PVDF	10 N	Not stated	30 V	[42]
Single-walled carbon nanotubes/PVDF	10 N	5.0 Hz	1 V	[35]
$NiFe_2O_4$/PVDF	10 N	20 Hz	0.156 V	[41]
ZnO_2–carbon nano-onions/PVDF	80 N	5.0 Hz	40 V	[39]
PVDF arrays	30 N	1.0 Hz	14 V	[43]
Polystyrene	*10 N*	*0.15 Hz*	*23.5 V*	*This work*

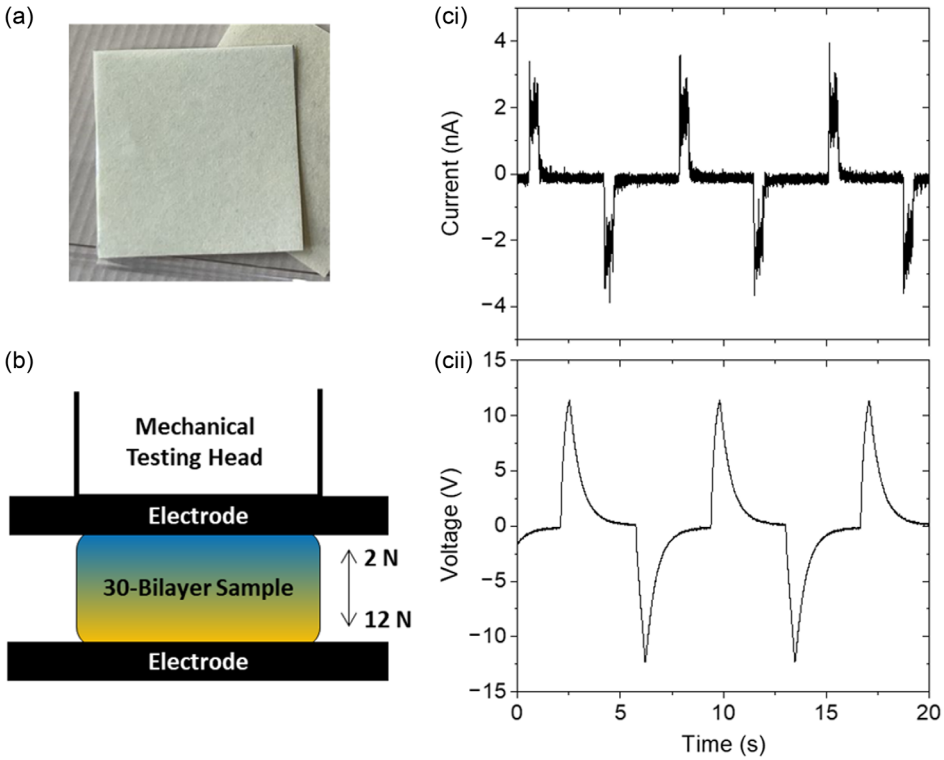

Figure 5. a) Photographs of as produced 30-bilayer rPS laminates (25 × 25 mm). b) Schematic of piezoelectric mode testing with applied compressive force from 2 up to 12 N with no break in contact between the mechanical testing head and the sample; c) piezoelectric mode testing data of a 30-bilayer rPS laminate; i) J_{sc} and ii) voltage measured across a 10 GΩ resistor.

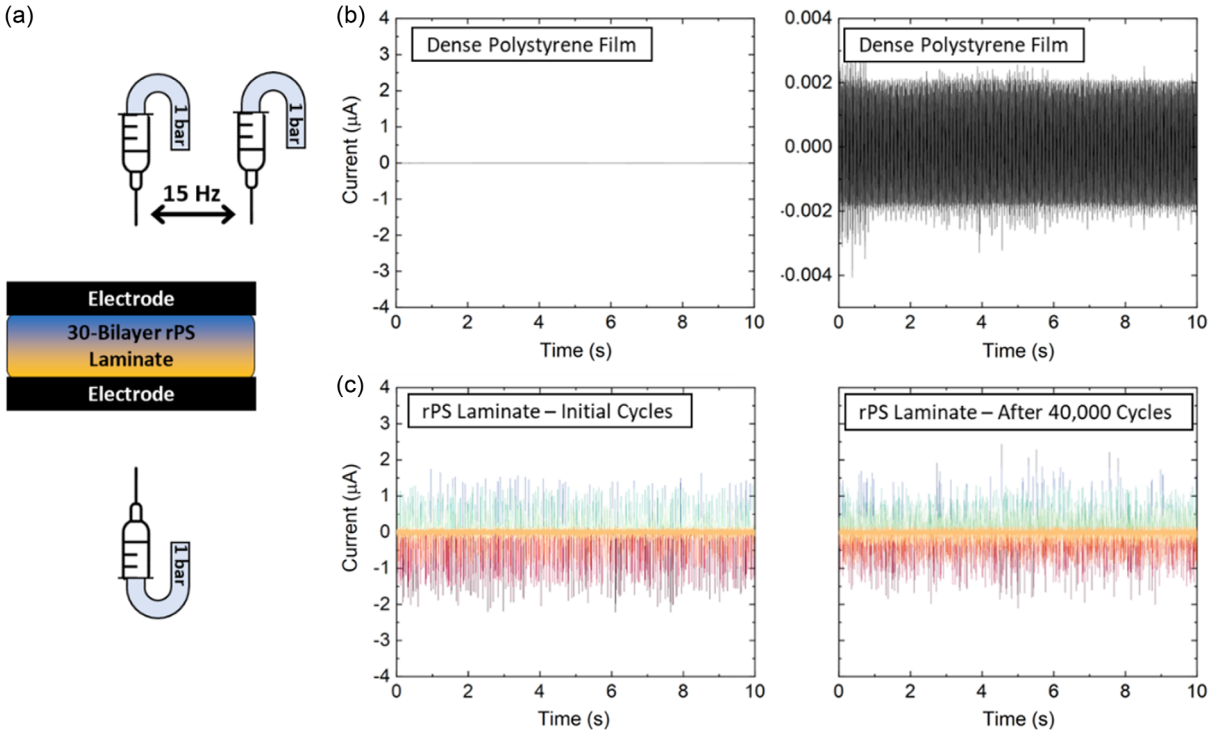

Figure 6. Energy harvesting from vibrations produced from air pressure changes; a) schematic of sample setup with a syringe blowing 1 bar of air onto the sample, the needle is oscillated at 14–15 Hz between the edge of the sample and the center with the current measured through the aluminum electrodes; b) negligible current measured from air pressure changes on a dense polystyrene film; and c) current measured from a 30-bilayer rPS laminate both initially and after 40 000 cycles.

While piezoelectric mode testing provides excellent characterization of the electromechanical response of the rPS laminate, to fully explore optimum energy-harvesting performance, TENG mode testing is required.

2.3. Electromechanical Performance: TENG Mode

Vertical contact-separation mode TENG testing was performed through contact-separation experiments between two individual laminate samples (**Figure 7**a,b).

By changing the electrospinning order, the contact interface between the two 30-bilayer samples was altered to demonstrate the importance of contact alignment (Figure 7c). These tests, performed in a precisely controlled manner with 0.1 m s^{-1} separation speed at 10 N maximum force, showed that by altering the contact interface from misaligned (large fiber vs large fiber or small fiber vs small fiber) to aligned (large fiber vs small fiber), an order of magnitude increase in current and voltage was observed (Figure 7c, S3, and S4, Supporting Information, and **Table 2**).

The aligned interface sample showed a peak-to-peak voltage of 135 ± 3 V (at 1 GΩ load resistance) and a I_{sc} of 268 ± 7 nA. This aligned interface can be considered analogous to using inversely polarized fluoropolymers in a TENG configuration.[48,49]

To demonstrate the full potential of rPS as a mechanical energy-harvesting material, contact-separation tests were performed at high speeds, up to 0.73 m s^{-1}, analogous to the walking speed of many patients requiring wearable electronics and sensors.[50] These tests resulted in an increase in measured peak-to-peak voltage to 200 ± 30 V and a further order of magnitude increase in I_{sc} up to $12\,000 \pm 500$ nA (Table 2, Figure S5, Supporting Information). This corresponds to a peak power density of 77.4 mW m^{-2} at a 100 MΩ load resistance (**Figure 8**a). Further, mechanical energy harvesting between two 30-bilayer rPS samples achieved charging of a 0.47 μF capacitor to 15 V in 200 s, reaching 1 V in 8 s (Figure 8b).

3. Conclusions

FPS presents a huge environmental issue in its disposal and recycling. Here, we have presented a simple pathway to reform PS into recycled polystyrene laminates with exceptional electromechanical responsiveness. These electrospun laminates are comparable to the state-of-the-art piezoelectric films when tested in contact mode showing minimal performance degradation at high frequency (36 Hz) operation over 24 h, generating a peak power of 77 mW m^{-2}, when operated in TENG mode. These structures provide an alternative electromechanically responsive polymer material to environmentally hazardous fluoropolymers.

4. Experimental Methods

Preparation of Electrospun Recycled PS Nanofibers and Laminates: To obtain an FPS solution (10 wt%), 1 g of FPS was dissolved in mixture

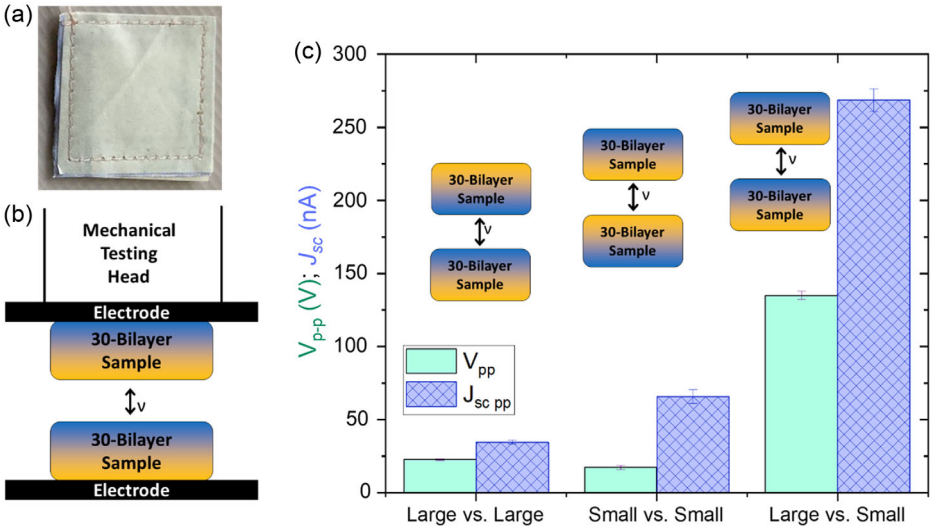

Figure 7. Vertical contact-separation TENG testing of 30-bilayer rPS laminates at 0.1 m s^{-1}; a) photograph of the 30-bilayer laminate with polyester-sewn border; b) schematic of the vertical contact-separation TENG mode testing configuration; and c) characterization of the peak-to-peak open-circuit voltage and the peak-to-peak short-circuit current for three configurations of the contact interface between the two individual 30-bilayer samples; large-diameter fibers contacting large-diameter fibers; small-diameter fibers contacting small-diameter fibers; and large-diameter fibers contacting small-diameter fibers.

Table 2. Comparison of electromechanical conversion from contact-separation between two 30-bilayer rPS laminates with different contact interfaces, tested in vertical contact-separation TENG mode.

Fiber contact interface	Separation speed [m s^{-1}]	Δ force [*N*]	V_{p-p} [V]	$I_{sc\ p-p}$ [nA]
Large versus large	0.1	10	22.6 ± 0.7	35 ± 1
Small versus small	0.1	10	17 ± 1	66 ± 5
Large versus small	0.1	10	135 ± 3	268 ± 7
Large versus small	0.73	16	200 ± 30	12 000 ± 500

of 1.215 mL THF and 8.345 mL DMF solution with the addition of 0.0338 g of sodium chloride (NaCl) and mixed at room temperature using a magnetic stirring at 500 rpm for 24 h. To obtain an FPS solution (30 wt%) 3 g of FPS was dissolved in a mixture of 0.954 mL THF and 6.490 mL DMF solution with the addition of 0.039 g of NaCl and mixed at room temperature using a magnetic stirring at 500 rpm for 24 h. The mixtures with 10 wt% and 30 wt% FPS were electrospun using needle electrospinning equipment at room temperature in constant ambient relative humidity (35%). The solutions were transferred to a 2 mL plastic syringe fitted with a needle (21 G, outer diameter 0.8 mm) and set up in the electrospinning apparatus. A grounded piece of aluminum foil was located 16 cm away from the capillary tip and used as a collector. The electric potential was controlled at 15 kV. For the FPS (10 wt%) solution, the flow rate was 0.1 mL h^{-1}, and for the FPS (30 wt%), the flow rate was 1.2 mL h^{-1}. The parameters to produce laminates of a given thickness are shown in **Table 3**.

Materials Characterization: Scanning Electron Microscopy: Scanning electron microscopy (SEM) of the rPS laminates was performed by sputter-coating a 4 nm gold layer onto the laminate surface, followed by imaging using an FEI Nova NanoSEM 650 field-emission SEM (The Netherlands) at an operating voltage of 5–10 kV. Samples were sputter-coated (Cressington 208HRD, Watford, UK) for 30 s using an Au target in an Ar atmosphere with a current of 80 mA, resulting in a 4 nm thick coating.

Materials Characterization: Cryo-Ion Mill and Helium Ion Microscopy: The rPS laminate cross sections were prepared by cryo-ion milling in a Leica

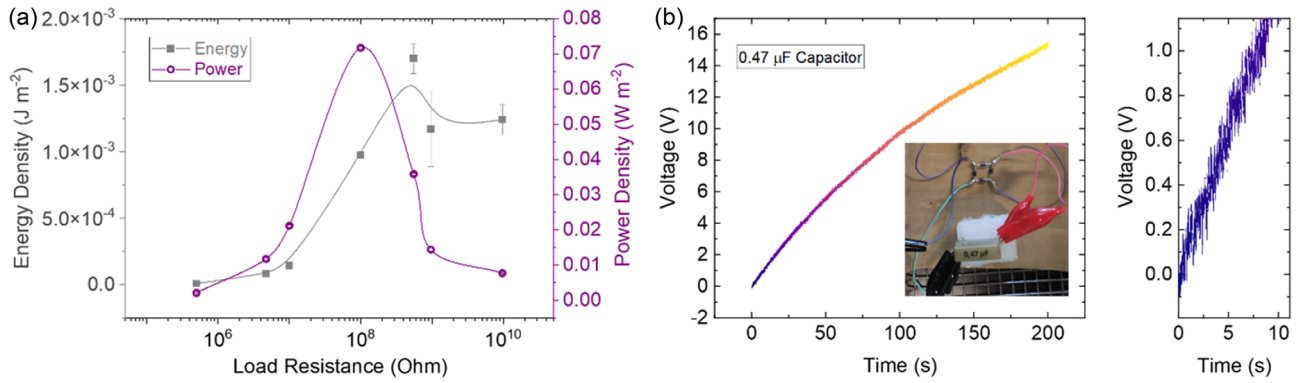

Figure 8. a) Power and energy calculations for a 30-bilayer rPS TENG; and b) charging a capacitor with 0.73 m s^{-1} separation speed between two aligned 30-bilayer rPS laminates; left: charging the capacitor fully; right: time to reach 1 V charge in the capacitor.

Table 3. Parameters for electrospinning rPS laminates.

Bilayer number	rPS solution [wt%]	Layer electrospinning time [min]	Layer thickness [μm]	Laminate thickness [μm]
1[a)]	10	416	≈100	≈200
	30	15	≈100	
3	10	208	≈50	≈300
	30	7.5	≈50	
15[a)]	10	12	≈5	≈150
	30	1.2	≈5	
30	10	12	≈5	≈300
	30	1.2	≈5	

[a)]Samples used for interfacial adhesion and microscopic characterization only, electromechanical characterization not shown.

EM TIC3X (Germany). Samples were mounted directly onto copper holders using copper adhesive tape and then cooled down to −150 °C before milling with a triple argon ion beam at 5 keV for 30 min. Helium ion microscopy (HIM) was performed on a Zeiss ORION NanoFab (Germany) using a 30 keV helium ion beam at a typical beam energy and current of 30 keV and 0.5 pA, respectively. No conductive coating was necessary for this imaging; instead, in situ charge neutralization by a low-energy electron flood gun was used.

Materials Characterization: Fiber Diameter Analysis: The average fiber diameter was calculated from the SEM images using the Gwyddion 2.53 software program (http://gwyddion.net/, Brno, Czech Republic). More than 100 fibers were counted from at least 3 SEM images which were taken from different places on a sample.

Materials Characterization: CARS: CARS was performed on an Olympus FV3000 laser-scanning confocal microscope (Japan) under femtosecond laser excitation. The tunable (792 nm, CARS pump wavelength) and fixed (1045 nm, CARS Stokes wavelength) outputs of a dual-output Ti:sapphire femtosecond laser (Spectra Physics InSight X3, USA) focused onto coverslip-mounted samples using a silicone-oil-immersion 30x objective with enhanced near-infrared transmittance (Olympus UPLSAPO30XSIR, Japan). The overlap between the pump and the Stokes beam was adjusted with a motorized delay line (Newport DL125, USA). Motorized variable attenuators were used to reduce the power of both beams to 10% of the laser output power. The backward (epi-) CARS signal at 638 nm, corresponding to the polystyrene Raman band at 3058 cm^{-1},[51] was optically filtered through short pass (690 SP) and band-pass (600/50) filters and collected with a time-correlated single photon counting detector (PicoQuant Hybrid PMA, Germany) synchronized with the excitation laser.

Interlayer Adhesion: Peel Testing: The 180° peel tests were performed on individual bilayers of small-diameter PS fibers electrospun on large-diameter PS fibers, and large-diameter PS fibers electrospun on small-diameter PS fibers with peeling at 100 mm min^{-1} and sample size 10 × 10 mm.

Electromechancial Testing: Piezoelectric Mode: The electromechanical response of triboelectric laminates (TLs) was tested using a dynamic test Instron E1000 instrument, which provided a constant pressing force and frequency. The samples were cut into pieces with dimensions of 1.5 × 1.5 cm. These samples were tested *via* cyclic compression at a frequency of 1 Hz, and with lower and upper force limits of 2 and 12 N. The V_{oc} and I_{sc} were measured using a Keithley 6514 electrometer (USA) connected to a PicoScope 5444B oscilloscope (UK). To eliminate friction,[34] the samples were adhered to indium-tin-oxide-coated glass slides using double-sided adhesive carbon tape (P77817-20, Science Services Gmb).

Electromechanical Testing: TENG Mode: The triboelectric measurements were made under controlled conditions—a separation distance of 5 mm, a pressing force of 10 N, and a contact-separation frequency of 1 Hz. To ensure repeatability, contact separation was carried out using an Instron E1000 material testing machine (USA). The generated current signals were measured using a Keithley 6514 electrometer (USA) connected to a PicoScope 5444B PC oscilloscope system (UK). For high-speed contact separation, a pneumatic device from custom-made programmable logic controller controlled (Mitsubishi AL2-24MR-D) the pneumatic system. A low friction smooth cylinder actuator (SMC MQML10) capable of producing 16 N contacting force and high translation speed (730 mm s^{-1}) was used, with a separation distance of 35 mm. A Faraday cage was placed around the triboelectric testing area to eliminate parasitic signals. All samples were measured in constant ambient relative humidity (35%).

Electromechanical Testing: Response to Airflow: To measure the electromechanical response to airflow, a custom testing rig was developed to vary air pressure incident on the PS laminates. This rig used two with an inner diameter of 1.5 mm with each nozzle was placed on different sides of the sample. One nozzle was stationary at 4 cm from the sample center while the other nozzle was moved from the sample center to 15 mm from the sample edge. The total displacement was 38 mm, at a frequency of 14–15 Hz. The moving nozzle was located 20 mm away from the sample surface. The laminate sample with attached Al electrode films was mounted in the plastic frame with an open area of 40 × 15 mm. The Al electrode, exposed to the moving nozzle, was perforated using a needle with a diameter of 0.3 mm. The hole density was 20 holes cm^{-2}.

Capacitor Charging: The AC signal from a TENG was rectified using a full bridge rectifier and then directed to a capacitor. The voltage across the capacitor was measured using a Keithley 6514 electrometer (USA) connected to a PicoScope 5444B PC oscilloscope (UK). Energy E (nJ), stored in the capacitor, was calculated using the Equation $E = 0.5CV^2$, where C is the capacitance of the capacitor (0.47 μF) and V is the voltage across the capacitor (V).

Supporting Information

Supporting Information is available from the Wiley Online Library or from the author.

Acknowledgements

The authors acknowledge funding by the Latvian Council of Science, project "Development of triboelectric laminates for energy harvesting by recycling waste polystyrene packaging," project no. lzp-2021/1–0603. P.C.S. and B.d.R. acknowledge support from RMIT University through the RMIT Vice-Chancellor's Research Fellowship program (2023). B.d.R.R. acknowledges support through the ARC LIEF scheme LE190100130. The authors would like to acknowledge the Materials Characterisation and Fabrication Platform (MCFP) and the Victorian Node of the Australian National Fabrication Facility (ANFF). The authors acknowledge the use of the Porous Microstructure Generator 2.0 for the preparation for Figure 4a (https://danielniblett.com/porous-microstructure-generator/).

Conflict of Interest

The authors declare no conflict of interest.

Author Contributions

Conceptualization: A.Š., P.C.S; Funding Acquisition: A.Š., B.d.R; Investigation: A.Š., H.D., B.d.R., M.I., K.M., A.L., A.B., R.T.L., P.C.S.; Methodology: A.Š., B.d.R., K.M., A.L., A.B., P.C.S.; Supervision: A.Š., A.V.E.; Visualization: A.Š., P.C.S, B.d.R.; Writing Original Draft: P.C.S.; Writing—Review & Editing: A.Š. A.Š., H.D., B.d.R., M.I., K.M., A.L., A.B., A.V.E., P.C.S.

Data Availability Statement

The data that support the findings of this study are available from the corresponding author upon reasonable request.

Keywords

energy harvestings, fibers, polystyrenes, recycled polymers, triboelectric nanogenerators, (TENGs)

Received: November 19, 2023
Revised: January 11, 2024
Published online: February 14, 2024

[1] P. Mishra, S. Vinayagam, K. Duraisamy, S. R. Patil, J. Godbole, A. Mohan, A. Mukherjee, N. Chandrasekaran, *Environ. Sci. Pollut. Res.* **2019**, *26*, 1537.
[2] C. Ingrao, A. L. Giudice, J. Bacenetti, A. M. Khaneghah, A. S. Sant'Ana, R. Rana, V. Siracusa, *Food Res. Int.* **2015**, *76*, 418.
[3] M. B. Hocking, *Science* **1991**, *251*, 504.
[4] B. T. Ho, T. K. Roberts, S. Lucas, *Crit. Rev. Biotechnol.* **2018**, *38*, 308.
[5] A. Šutka, L. Lapčinskis, D. He, H. Kim, J. D. Berry, J. Bai, M. Knite, A. V. Ellis, C. K. Jeong, P. C. Sherrell, *Adv. Mater. Interfaces* **2023**, *10*, 2300323.
[6] G. Energy, in *CO2 Status Report*, IEA (International Energy Agency), Paris, France **2019**.
[7] M. T. García, G. Duque, I. Gracia, A. de Lucas, J. F. Rodríguez, *J. Mater. Cycles Waste Manage.* **2009**, *11*, 2.
[8] C. Marquez, C. Martin, N. Linares, D. De Vos, *Mater. Horiz.* **2023**, *10*, 1625.
[9] T. Maharana, Y. S. Negi, B. Mohanty, *PPTEn* **2007**, *46*, 729.
[10] N. Chaukura, W. Gwenzi, T. Bunhu, D. T. Ruziwa, I. Pumure, *Resour. Conserv. Recycl.* **2016**, *107*, 157.
[11] J. Curry, N. Harris, *Sensors* **2019**, *19*, 1940.
[12] A. Corletto, A. V. Ellis, N. A. Shepelin, M. Fronzi, D. A. Winkler, J. G. Shapter, P. C. Sherrell, *Adv. Mater.* **2022**, *34*, 2203849.
[13] N. D. Tyrrell, *Org. Process Res. Dev.* **2023**, *27*, 1422.
[14] R. Lohmann, I. T. Cousins, J. C. DeWitt, J. Gluge, G. Goldenman, D. Herzke, A. B. Lindstrom, M. F. Miller, C. A. Ng, S. Patton, *Environ. Sci. Technol.* **2020**, *54*, 12820.
[15] J. Gardiner, *Aust. J. Chem.* **2014**, *68*, 13.
[16] A. Ahmed, Z. Saadatnia, I. Hassan, Y. Zi, Y. Xi, X. He, J. Zu, Z. L. Wang, *Adv. Energy Mater.* **2017**, *7*, 1601705.
[17] J. Xiong, P. Cui, X. Chen, J. Wang, K. Parida, M.-F. Lin, P. S. Lee, *Nat. Commun.* **2018**, *9*, 4280.
[18] A. Ahmed, I. Hassan, A. S. Helal, V. Sencadas, A. Radhi, C. K. Jeong, M. F. El-Kady, *Iscience* **2020**, *23*, 101286.
[19] F.-R. Fan, Z.-Q. Tian, Z. L. Wang, *Nano Energy* **2012**, *1*, 328.
[20] G. Grosjean, S. Wald, J. C. Sobarzo, S. Waitukaitis, *Phys. Rev. Mater.* **2020**, *4*, 082602.
[21] S. R. Waitukaitis, V. Lee, J. M. Pierson, S. L. Forman, H. M. Jaeger, *Phys. Rev. Lett.* **2014**, *112*, 218001.
[22] L. Lapčinskis, A. Linarts, K. Mālnieks, H. Kim, K. Rubenis, K. Pudzs, K. Smits, A. Kovaļovs, K. Kalniņš, A. Tamm, C. K. Jeong, A. Šutka, *J. Mater. Chem. A* **2021**, *9*, 8984.
[23] O. Verners, L. Lapčinskis, L. Ģermane, A. Kasikov, M. Timusk, K. Pudzs, A. V. Ellis, P. C. Sherrell, A. Šutka, *Nano Energy* **2022**, *104*, 107914.
[24] L. Lapčinskis, L. Ģērmane, O. Platnieks, A. Krikovs, S. Gaidukovs, K. Pudzs, A. Linarts, P. C. Sherrell, A. Šutka, *Adv. Sustain. Syst.* **2023**, *7*, 2300280.
[25] M. M. Apodaca, P. J. Wesson, K. J. Bishop, M. A. Ratner, B. A. Grzybowski, *Angew. Chem. Int. Ed.* **2010**, *49*, 946.
[26] A. Linarts, P. C. Sherrell, K. Mālnieks, A. V. Ellis, A. Šutka, *Small* **2023**, *19*, 2205563.
[27] K. Mālnieks, P. Kaufelde, A. Linarts, L. Lapčinskis, O. Verners, A. Šutka, *Mater. Lett.* **2022**, *329*, 133188.
[28] P. C. Sherrell, A. Sutka, N. A. Shepelin, L. Lapcinskis, O. Verners, L. Germane, M. Timusk, R. A. Fenati, K. Malnieks, A. V. Ellis, *ACS Appl. Mater. Interfaces* **2021**, *13*, 44935.
[29] J. Park, S. Jo, Y. Kim, S. Zaman, D. Kim, *Micromachines* **2022**, *13*, 380.
[30] A. Babu, I. Aazem, R. Walden, S. Bairagi, D. M. Mulvihill, S. C. Pillai, *Chem. Eng. J.* **2023**, *452*, 139060.
[31] U. Stachewicz, C. A. Stone, C. R. Willis, A. H. Barber, *J. Mater. Chem.* **2012**, *22*, 22935.
[32] A. Šutka, K. Mālnieks, L. Lapčinskis, M. Timusk, K. Kalniņš, A. Kovaļovs, J. Bitenieks, M. Knite, D. Stevens, J. Grunlan, *Phys. Chem. Chem. Phys.* **2020**, *22*, 13299.
[33] C. Xu, B. Zhang, A. C. Wang, H. Zou, G. Liu, W. Ding, C. Wu, M. Ma, P. Feng, Z. Lin, Z. L. Wang, *ACS Nano* **2019**, *13*, 2034.
[34] A. Šutka, P. C. Sherrell, N. A. Shepelin, L. Lapčinskis, K. Mālnieks, A. V. Ellis, *Adv. Mater.* **2020**, *32*, 2002979.
[35] N. A. Shepelin, P. C. Sherrell, E. Goudeli, E. N. Skountzos, V. C. Lussini, G. W. Dicinoski, J. G. Shapter, A. V. Ellis, *Energy Environ. Sci.* **2020**, *13*, 868.
[36] N. A. Shepelin, A. M. Glushenkov, V. C. Lussini, P. J. Fox, G. W. Dicinoski, J. G. Shapter, A. V. Ellisv, *Energy Environ. Sci.* **2019**, *12*, 1143.
[37] Y. Su, W. Li, X. Cheng, Y. Zhou, S. Yang, X. Zhang, C. Chen, T. Yang, H. Pan, G. Xie, G. Chen, X. Zhao, X. Xiao, B. Li, H. Tai, Y. Jiang, L.-Q. Chen, F. Li, J. Chen, *Nat. Commun.* **2022**, *13*, 4867.
[38] H. Pei, J. Jing, Y. Chen, J. Guo, N. Chen, *Nano Energy* **2023**, *109*, 108303.
[39] Y. Khazani, E. Rafiee, A. Samadi, *Colloids Surf., A* **2023**, *675*, 132004.
[40] W. Qin, P. Zhou, X. Xu, M. S. Irshad, Y. Qi, T. Zhang, *Sens. Actuators A Phys.* **2022**, *333*, 113307.
[41] L. Paralı, Ç. E. Demirci Dönmez, M. Koç, S. Aktürk, *CAP* **2022**, *36*, 143.
[42] N. P. Maria Joseph Raj, A. Ks, G. Khandelwal, S.-J. Kim, *Sustain. Energy Fuels* **2022**, *6*, 674.
[43] L. He, J. Lu, C. Han, X. Liu, J. Liu, C. Zhangv, *Small* **2022**, *18*, 2200114.
[44] S. Sahoo, K. Krishnamoorthy, P. Pazhamalai, V. K. Mariappan, S. Manoharan, S.-J. Kimv, *J. Mater. Chem. A* **2019**, *7*, 21693.
[45] Y. Zhang, Y. Zhang, X. Xue, C. Cui, B. He, Y. Nie, P. Deng, Z. Lin Wangv, *Nanotechnology* **2014**, *25*, 105401.
[46] Y. Xue, T. Yang, Y. Zheng, K. Wang, E. Wang, H. Wang, L. Zhu, Z. Du, H. Wang, K.-C. Chou, X. Houv, *Adv. Sci.* **2023**, *10*, 2300650.
[47] R. T. Leon, P. C. Sherrell, A. Šutka, A. V. Ellis, *Nano Energy* **2023**, *110*, 108445.
[48] A. Šutka, K. Mālnieks, A. Linarts, M. Timusk, V. Jurķāns, I. Gorņevs, J. Blūms, A. Bērziņa, U. Joost, M. Knite, *Energy Environ. Sci.* **2018**, *11*, 1437.
[49] A. Šutka, K. Mālnieks, A. Linarts, P. C. Sherrell, X. Yu, E. Bilotti, *ACS Appl. Energy Mater.* **2023**, *6*, 9300.
[50] N. M. Peel, S. S. Kuys, K. Klein, *J. Gerontol. Series A* **2012**, *68*, 39.
[51] A. D. Curtis, A. R. Calchera, M. C. Asplund, J. E. Patterson, *Vib. Spectrosc.* **2013**, *68*, 71.
[52] J. Zhou, B. Del Rosal, D. Jaque, S. Uchiyama, D. Jin, *Nat. Methods* **2020**, *17*, 967.
[53] A. Zumbusch, G. R. Holtom, X. S. Xie, *Phys. Rev. Lett.* **1999**, *82*, 4142.